JOURNAL OF MATERIALS SCIENCE 17 (1982) 1807–1818

Application of surface behaviour diagrams to the study of hydration of phosphoric acid-anodized aluminium

G. D. DAVIS, T. S. SUN, J. S. AHEARN, J. D. VENABLES
Martin Marietta Corporation, Martin Marietta Laboratories, 1450 South Rolling Road, Baltimore, Maryland 21227, USA

The hydration of aluminium surfaces prepared for adhesive bonding by anodization in phosphoric acid has been studied using surface behaviour diagrams. These surface behaviour diagrams, which are similar to phase diagrams for equilibrium bulk phases, trace the evolution of the aluminium adherend surface composition, obtained by X-ray photoelectron spectroscopy, during the hydration process. When supplemented with high-resolution scanning electron micrographs and Auger depth profiles, the surface behaviour diagrams show that hydration proceeds in three steps. The first step is reversible and consists of the adsorption of water by the monolayer of $AlPO_4$ initially present on the surface. It involves no change in the oxide morphology. The second, which appears to be rate-controlling, involves the slow dissolution of the phosphate followed by rapid hydration of the exposed alumina to the oxyhydroxide, boehmite. During this stage, extensive morphological changes occur as the boehmite fills the pore cells and bridges the whiskers of the original surface. The third step consists of the nucleation and growth of the trihydroxide, bayerite, on top of the boehmite. Using these results as examples, we propose the surface behaviour diagram approach as a new tool for the study of surface reactions in general.

1. Introduction

During the last four years, investigators at Martin Marietta Laboratories have conducted a comprehensive investigation to determine the factors responsible for promoting the integrity and long-term durability of adhesively-bonded aluminium structures. Two extremely important concepts have evolved from this work. First, it has been clearly demonstrated that the microscopic roughness of the oxide surface on Al is the single most critical factor in determining initial bond strength [1]. Rough and porous oxides are produced by various etching and anodizing pre-treatment processes, such as the Forest Products Laboratory (FPL) sulphuric acid–sodium dichromate etch [2], phosphoric acid anodization (PAA) [3], and chromic acid anodization (CAA) [4]. The rough surface is important because it mechanically interlocks with the overlying polymer to form a much stronger bond than is possible with a smooth oxide.

The second important finding is that the long-term durability of aluminium–polymer bonds is determined almost exclusively by the degree of stability of the aluminium oxide in a humid environment [5]. Moisture transforms the oxide to a hydroxide with an accompanying morphological change. The resulting material, the boehmite form of aluminium hydroxide, adheres poorly to the aluminium beneath it. Therefore, once it forms, the overall bond strength is severely degraded.

In the past year, we have conducted work in order to try to understand the oxide-to-hydroxide conversion process on aluminium. One of the techniques that has been developed to study this problem is discussed here in detail. In brief, X-ray photoelectron spectroscopy (XPS) [also known as electron spectroscopy for chemical analysis (ESCA)] has been used to provide data for generating surface behaviour diagrams. This type of diagram, which is similar to a phase diagram for

0022–2461/82/061807–12$03.94/0

equilibrium bulk phases, is a convenient and potentially very powerful technique for tracing the evolution of surface reactions and the stability of adsorbed species. As far as we know, this is the first time such an approach has been used in the study of surfaces and we suggest that it may be an approach applicable for a wide range of applications in the surface science field.

The present study covers our investigations into the stability of aluminium surfaces that have been treated with the PAA process. Our objective was to determine why the PAA oxide is more stable in a humid environment than oxides produced by other adhesive bonding procedures.

2. Experimental techniques

The X-ray photoelectron spectroscopy measurements were carried out using a Physical Electronics spectrometer (Model 548) featuring a double-pass cylindrical mirror analyser (CMA) capable of Auger-electron spectroscopy (AES), X-ray photoelectron spectroscopy (XPS) and ultra-violet photoelectron spectroscopy (UPS). Several important features of this spectrometer have been previously reported [6–8]. The X-ray source, which contains a Mg anode, has a characteristic $K\alpha$ line at 1253.6 eV, and a line-width of 0.6 eV without monochromatization. The energy resolution of the analyser was set at ~4.0 eV for panoramic scans (with binding energies of 0 to 1000 eV) and at ~1.0 eV for individual peak analyses (with 10 to 20 eV ranges of binding energies). The high-resolution spectra were used to obtain line intensities and to determine peak positions.

The intensity of an XPS line was calculated from the area under the peak after a linear background subtraction. To perform quantitative analysis, the sensitivity factors of the major XPS lines, Al 2p, P 2p, and O 1s, were determined from the spectra of high-purity powders of α-Al_2O_3, γ-Al_2O_3, $AlPO_4$, and Na_3PO_4. As indicated in Table I, the sensitivity factors (normalized with respect to oxygen) agree fairly well with the published values [9]. The relative elemental concentrations of a surface were determined from the intensities of the XPS lines of the various elements divided by the appropriate sensitivity factors and then normalized so that the total concentration of the individual elements added to 100%.

TABLE I XPS sensitivity factors

Element	XPS line	This work	Data from [9]
O	1s	1.0	1.0
Al	2p	0.20	0.17
P	2p	0.51	0.40

The binding energy scale of the spectrometer was calibrated with reference to the Au $4f_{7/2}$ and C 1s peaks at 83.8 and 285.0 eV, respectively. However, since charging of non-conducting surfaces may shift observed binding energies uniformly, only differences in binding energies are reported.

Oxide morphology and hydrate structure were studied with a JEOL 100CX scanning transmission electron microscope (STEM), operated in the high-resolution scanning mode. The details of STEM specimen preparation were described in a previous study [1]. To improve the topographic perception of the surface structures, stereo pairs were made (10° tilt angle) of all the micrographs.

The specimen strips (1 cm x 8 cm) were made from sheets of commercial 2024-T3 Al alloy with a nominal composition of 93.5 wt% Al, 4.4 wt% Cu, 1.5 wt% Mg, and 0.6 wt% Mn. They were pretreated with the Forest Products Laboratory (FPL) process, [2] which consists of de-greasing, alkaline cleaning and etching in a solution containing $Na_2Cr_2O_7 \cdot 2H_2O$, H_2SO_4, and H_2O in a 1:10:30 ratio by weight. After a thorough rinse, the specimens were anodized for 20 min in an aqueous solution of 10 wt% H_3PO_4 at +10 V with respect to a Pt counter-electrode. The anodized specimens were rinsed with distilled water or, in some cases, with acetone, dried with warm air, and stored in a vacuum desiccator at room temperature.

The anodization produced an oxide film consisting of a thin (10 nm) barrier layer adjacent to the metal and a thick (~400 nm) porous layer at the top. The present authors have investigated several important characteristics of the oxide film [1, 5, 6, 10, 11]. The porous layer consists of a thin barrier layer underneath closely-packed pore cells, with fine whiskers at the top. Fig. 1 shows stereo electron micrographs and an isometric drawing of the oxide morphology from a fresh specimen. The anodic oxide is composed predominantly of amorphous Al_2O_3. The major components of the alloy, Cu, Mg and Mn, are not present in the oxide within the limit of the XPS detection (~0.1%).

Identically prepared PAA-Al coupons were exposed to air (at either 50 or 60° C) saturated with water vapour (100% relative humidity) in a Blue M temperature-controlled humidity chamber.

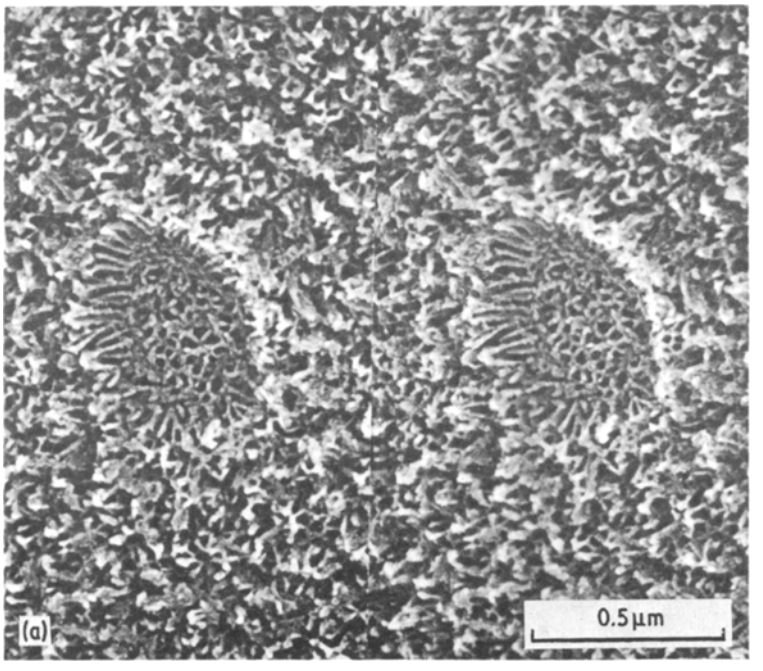

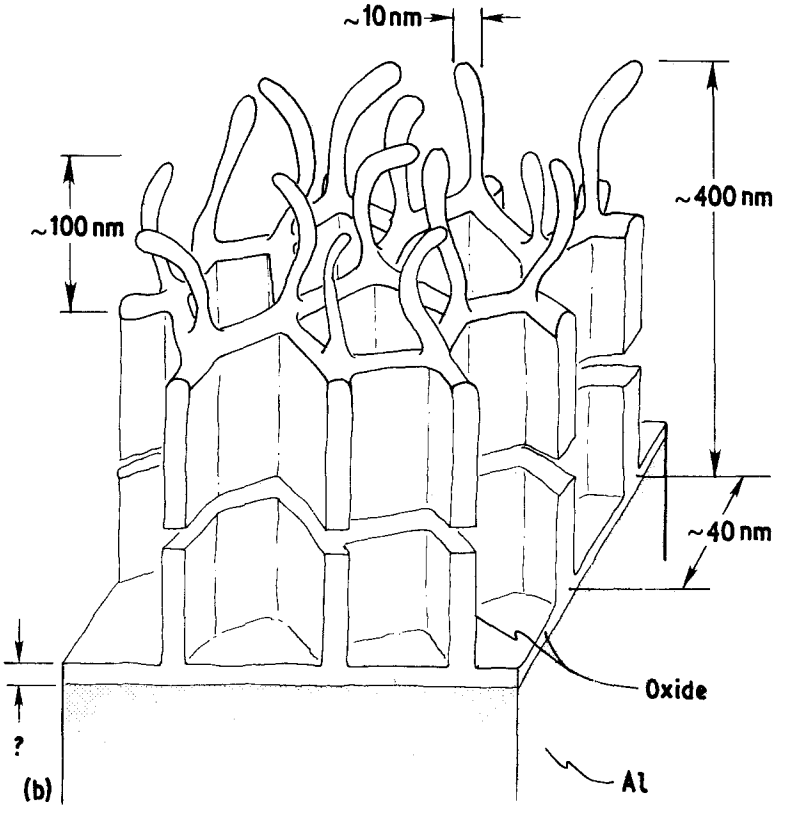

Figure 1 (a) Ultra-high resolution stereo micrograph and (b) isometric drawing of the oxide morphology on a PAA-treated aluminium surface. The origin of the depressed region in the oxide seen in (a) is unknown, but may have been due to a gas bubble that inhibited oxide growth ([1]).

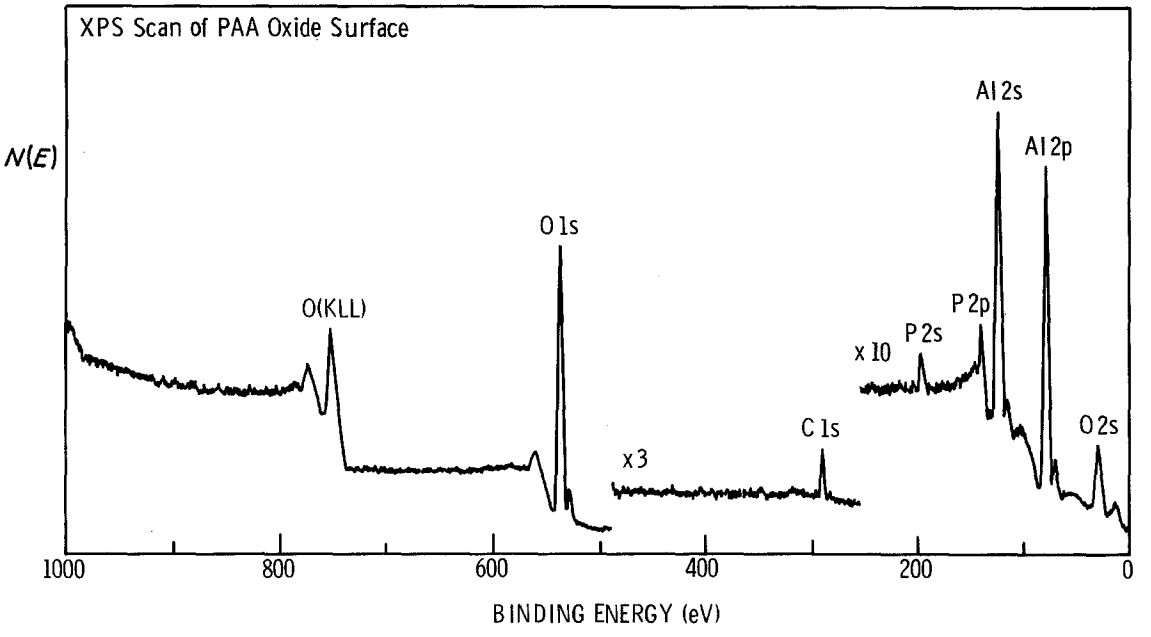

Figure 2 The X-ray photoelectron spectrum of a freshly-prepared PAA–Al oxide surface.

The samples were suspended vertically so that condensation could drop off. The specimens were removed from the humid environment at different intervals, dried with forced air at room temperature, and stored in a desiccator prior to measurement with the STEM or the XPS spectrometer.

3. Results

3.1. Chemical information from XPS

A typical XPS spectrum of the PAA oxide is shown in Fig. 2. Only four elements, Al, P, C, and O, are present on the surface. This result is consistent with that of a previous study based on Auger electron spectroscopy [10]. According to the Auger depth profiles, the hydrocarbon species is present only on the surface layer and is attributed to contamination. Based on the binding energy differences of their XPS lines, the chemical states of Al and P are identified as those of Al_2O_3 and a phosphate, presumably $AlPO_4$, respectively (see Table II). Any excess oxygen, indicated by quantitative analysis, is assumed to be bonded to hydrogen, which cannot be detected directly by XPS, but which has been detected by infra-red spectroscopy [12, 13]. Since the hydration products of Al_2O_3, AlOOH and $Al(OH)_3$, can be written in the form $Al_2O_3 \cdot nH_2O$, the surface composition can be represented as a linear combination of Al_2O_3, $AlPO_4$, and H_2O.

TABLE II Binding-energy differences for several Al- and P-containing compounds

Sample	Binding-energy differences (eV)	
	(O 1s to Al 2p)	(O 1s to P 2p)
PAA surface	456.2 ± 0.4	396.7 ± 0.4
$AlPO_4$	456.4 ± 0.4	397.2 ± 0.4
Na_3PO_4		397.1 ± 0.4
Al_2O_3	456.0 ± 0.4	
$Al(OH)_3$	456.9 ± 0.4	

3.2. The surface behaviour diagram

The elementary composition defined from XPS measurements can be converted into a ternary composition $xAl_2O_3 + yAlPO_4 + zH_2O$. The measured intensity of the O 1s peak is assumed to be the total of the contributions from oxygen in Al_2O_3, $AlPO_4$, and H_2O. These two systems are related to each other through the following equations:

$$x = K(C_{Al} - C_P); \quad (1)$$

$$y = 2KC_P; \quad (2)$$

and

$$z = K(2C_O - 3C_{Al} - 5C_P) = 1 - x - y, \quad (3)$$

where C is the relative atomic concentration of the element denoted by the subscript and $K = \frac{1}{2}(C_O - C_{Al} - 2C_P)^{-1}$, a normalization factor. Each composition can be plotted as a point, (x, y, z), in the surface behaviour diagram, as shown in Fig. 3. The

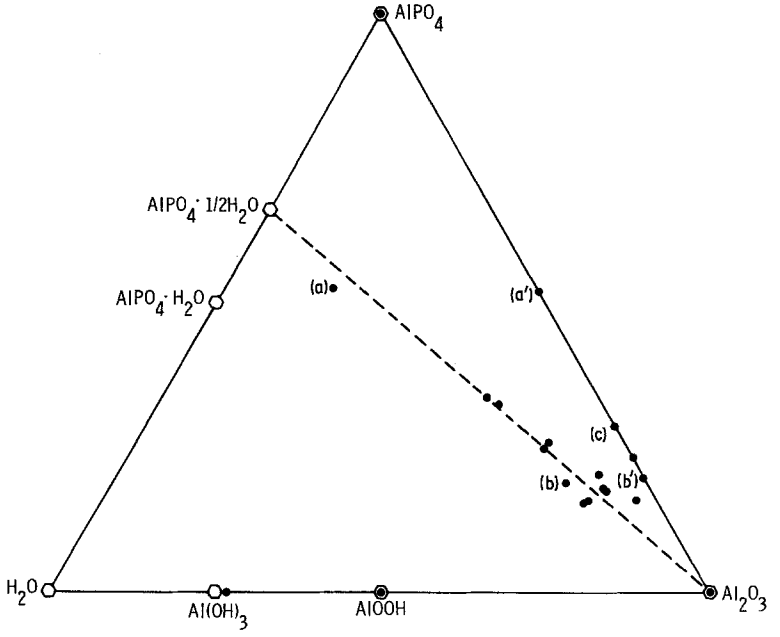

Figure 3 The $AlPO_4$–Al_2O_3–H_2O surface behaviour diagram of the fresh PAA–Al oxide surface, as determined by XPS measurements. The solid points are experimental compositions. The open points are calculated compositions. All surfaces were rinsed in water after anodization. Points a and a′ and b and b′ represent the same coupon before and after dehydration in an ultra-high vacuum chamber (see text).

results for several known compounds and the PAA oxide specimens prepared under different conditions are shown in the behaviour diagram and are discussed below.

Since the data obtained from Al_2O_3 and $AlPO_4$ were used as reference standards to determine the sensitivity factors of the elements, their experimental and calculated compositions are, by definition, identical. However, the agreement between the measured and calculated compositions of the two aluminium hydroxides, AlOOH and $Al(OH)_3$, validates the sensitivity factors used in this work.

3.3. The initial oxide surface

The compositions of the PAA oxides lie between two tie-lines: $AlPO_4$–Al_2O_3 and $AlPO_4 \cdot \frac{1}{2}H_2O$–$Al_2O_3$. The large variation in the $AlPO_4$ to Al_2O_3 ratios is attributed mainly to differences in the post-anodization rinse conditions. For example, coupons rinsed with acetone rather than water exhibited much higher phosphate concentrations and little, if any, detectable Al_2O_3. The $AlPO_4$ concentrations observed on water-rinsed surfaces ranged up to about 53% (see Points a and a′ in Fig. 3), with the majority clustering at about 20%, a value corresponding to a monolayer of $AlPO_4$ on top of the Al_2O_3 substrate (assuming that the mean free-path of the P 2p and Al 2p photoelectrons is 1.6 nm [14] and the average thickness of one $AlPO_4$ layer is about 0.4 nm.

The majority of the PAA specimens exhibit some degree of hydration, i.e., $z \neq 0$, due to the presence of the $AlPO_4 \cdot nH_2O$, ($n \leqslant 1$). However, dehydration occurred readily in vacuum, as illustrated by two pairs of data points a–a′ and b–b′ in Fig. 3. The unprimed entries represent the surface compositions shortly after the coupons were placed in the ultra-high vacuum (UHV) chamber and the primed entries represent the compositions for the same specimens after they were kept in the vacuum for three days. The latter points indicate a nearly total reduction of water content. Data from another specimen, c, kept in a vacuum desiccator for 50 days before transfer to the UHV chamber, also exhibited an unhydrated state. The scatter in composition along the horizontal direction is, therefore, attributed primarily to the storage conditions of the specimens. As a general rule, the longer the specimens were stored in vacuo, the closer the composition to the $AlPO_4$–Al_2O_3 tie-line. Furthermore, the oxide morphology (as observed in the STEM) within each group of identically anodized specimens is not detectably different, despite the variation in water content. These results suggest that the initial hydration stage is reversible, involving the adsorption of water by the $AlPO_4$ on the surface.

3.4. Evolution of surface composition during hydration

The results for a series of specimens that were

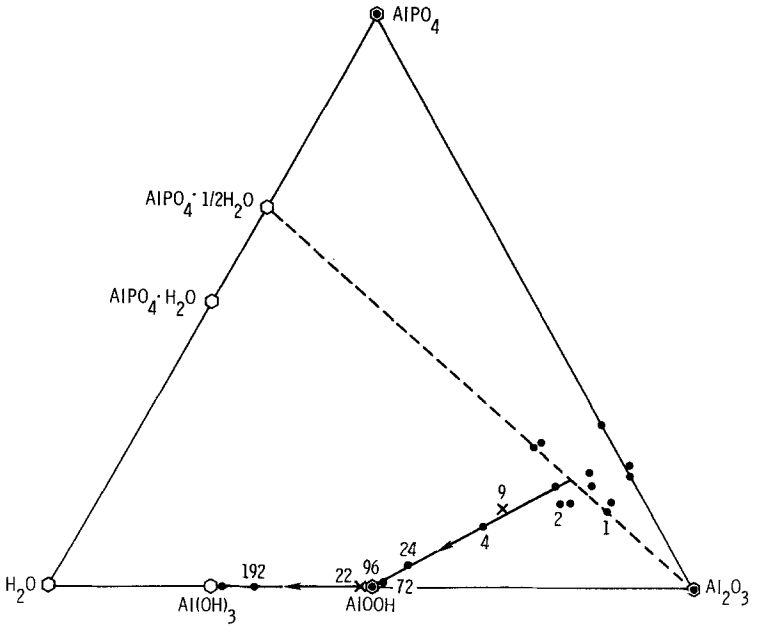

Figure 4 The surface behaviour diagram of fresh and hydrated PAA–Al oxide surfaces. The numbers by some of the points denote the exposure in hours to 100% relative humidity at 50° C (solid points) or at 60° C (crosses).

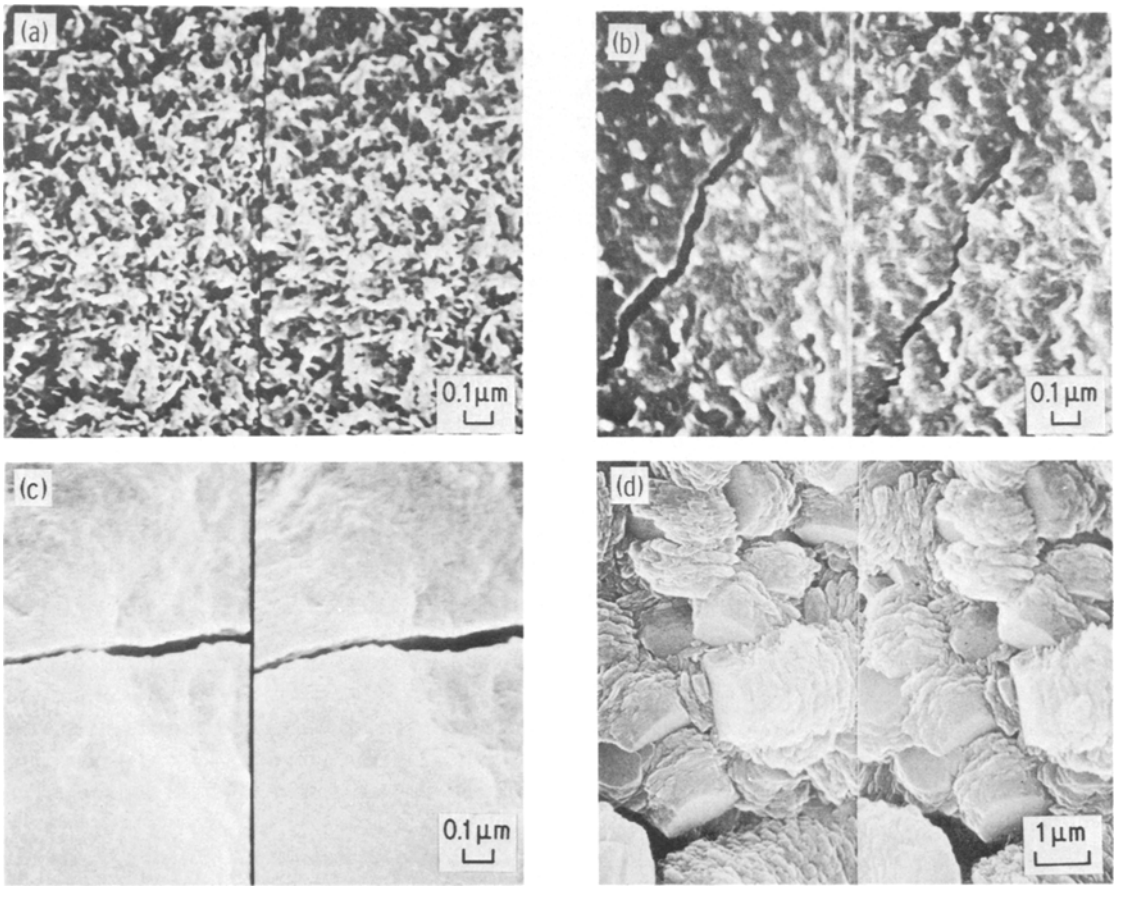

Figure 5 Stereo SEM micrographs of PAA–Al oxide samples after exposure to 100% relative humidity at 50° C for (a) 4 h, (b) 24 h, (c) 72 h, and (d) 192 h.

prepared identically but exposed to 100% relative humidity at 50° C for various lengths of time are shown in the behaviour diagram shown in Fig. 4. The exposure time (in h) is indicated by the number adjacent to each data point. For comparison, the corresponding stereo micrographs of four of these specimens are shown in Fig. 5.

With one- and two-hour exposures, the H_2O concentration on the specimen surface increased slightly, but the composition remained near the $AlPO_4 \cdot \frac{1}{2}H_2O$–$Al_2O_3$ tie-line. No change of oxide morphology was seen for these samples, indicating that the hydration activity at this early stage was confined to the first few atomic layers and probably involved the adsorption of water by the $AlPO_4$, as mentioned earlier.

When the exposure was increased from 2 to 4 h, the surface composition evolved away from the $AlPO_4 \cdot \frac{1}{2}H_2O$–$Al_2O_3$ tie-line. New structures, presumably some hydration product, appeared to grow around the whiskers, forming bridges between them, and, in some cases, covering the pores (Fig. 5). This stage marks the beginning of a more drastic hydration activity.

As the humidity exposure is increased further, the H_2O-content increases at the expense of both the Al_2O_3 and $AlPO_4$ contents. The composition changed steadily along a straight line until it reached AlOOH (boehmite) at 96-h exposure. From this point on, further exposure caused the composition to change along the Al_2O_3–H_2O tie-line toward the most advanced hydration state, i.e., $Al(OH)_3$ (bayerite), as indicated by the point for the specimen exposed for 192 h (see Fig. 4).

The corresponding electron micrographs (see Fig. 5) show that the hydration product nearly fills up the pores at 24-h exposure and grows to an over-layer at 72 h. Electron diffraction analyses made at both stages revealed the structure of a boehmite phase that corresponded with the composition data obtained with XPS. When the exposure is increased to 192 h, crystallites of a second hydration product covered the specimen surface (see Fig. 5d). An X-ray diffraction analysis on the layer covering this specimen revealed both bayerite and boehmite structures, with the first one dominant, i.e., a layer of bayerite has grown on top of the boehmite. These results are consistent with those of Vedder and Vermilyea [12, 15] who used bulk-sensitive techniques and reported the formation of a pseudo-boehmite phase with a water content between that of boehmite and bayerite.

A second hydration experiment was performed at 60° C at 100% relative humidity. The hydration process again followed the same tie-line shown in the behaviour diagram in Fig. 4. In general, less time was required for the hydration to occur at 60° C than was necessary at 50° C, but there was considerable variation from sample to sample and across the same sample. We can correlate these

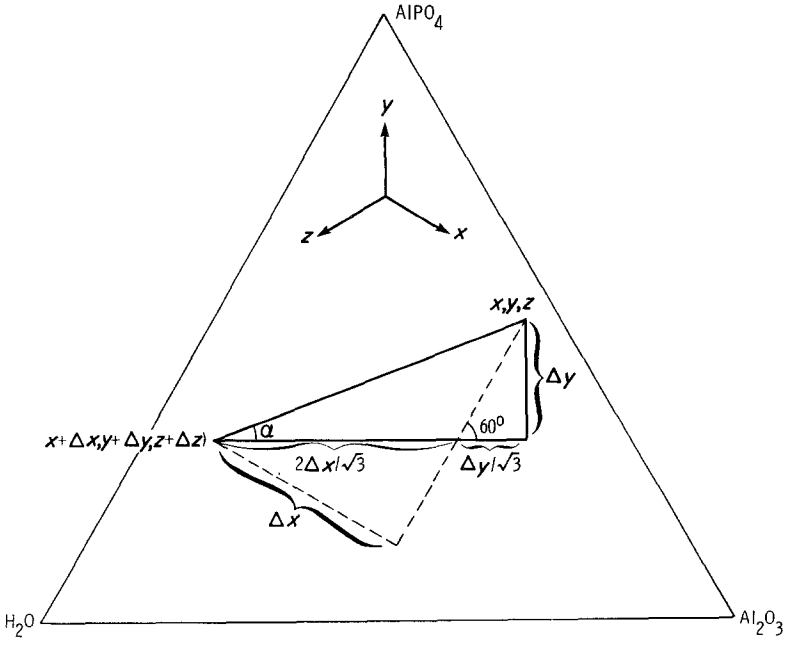

Figure 6 Surface behaviour diagram illustrating the derivation of Equation 4.

variations with non-uniformities in phosphate coverage; the greater the phosphate concentration, the longer the time to achieve hydration [16].

4. Model of hydration process

To help develop a model for the hydration process, the expected surface composition changes were compared with the experimental results for the various possible reactions.

The initial specimen composition at a given stage is defined as $xAl_2O_3 + yAlPO_4 + zH_2O$, i.e., at the position (x, y, z) in the behaviour diagram. At some small time interval later, the concentration changes to a new position $(x + \Delta x,\ y + \Delta y,\ z + \Delta z)$, where $\Delta x + \Delta y + \Delta z = 0$ (see Fig. 6). The direction of evolution is described by the angle, α, between the line connecting (x, y, z) and $(x + \Delta x, y + \Delta y, z + \Delta z)$ and the horizontal axis. It can be shown by trigonometric construction that:

$$\tan\alpha = \frac{\sqrt{3}}{1 + 2\Delta x/\Delta y}. \qquad (4)$$

This equation allows us to determine the direction of evolution with respect to the following possible reactions.

4.1. Hydration of surface $AlPO_4$ to form $AlPO_4 \cdot nH_2O$

In this case, the $AlPO_4$ content does not change significantly, whereas the content of H_2O increases at the expense of detectable Al_2O_3, i.e., $\Delta z > 0$, $\Delta y \simeq 0$, and $\Delta x \simeq -\Delta z$. It follows that $\tan\alpha \simeq 0$ and $\alpha \simeq 0$. Thus, the surface composition evolves along the horizontal direction (Path a in Fig. 7). The dehydration of $AlPO_4 \cdot nH_2O$ proceeds in the same way, but in the reverse direction.

This behaviour can also be generalized to a surface containing no phosphate. The surface Al_2O_3 becomes hydrated and less of the underlying Al_2O_3 is detected. The composition then follows the Al_2O_3–H_2O tie-lie (Path a′ in Fig. 7).

4.2. Nucleation and growth of a hydrated phase with composition $Al_2O_3 \cdot nH_2O$

Phenomenologically, the surface coverage of $Al_2O_3 \cdot nH_2O$ increases with time at the expense of the original surface composition. The new surface composition can be expressed as

$$\delta Al_2O_3 \cdot nH_2O + (1 - \delta')(xAl_2O_3 + yAlPO_4 + zH_2O),$$

where δ denotes the increment of the hydrated phase and δ' denotes the corresponding decrement of the original surface constituents. Thus, $\Delta x = \delta - x\delta'$, $\Delta y = -y\delta'$, and $\Delta z = n\delta - z\delta'$. The requirement that $\Delta x = \Delta y + \Delta z = 0$ implies that $\delta' = (n + 1)\delta$. Therefore, $\Delta x = [1 - x(n + 1)]\delta$,

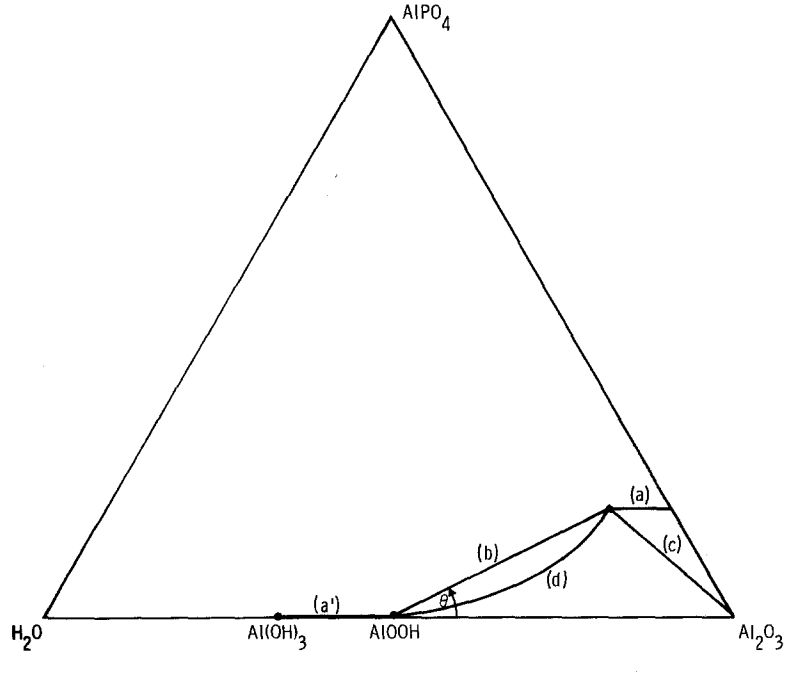

Figure 7 The surface behaviour diagram showing different evolution paths of surface composition: (a) hydration of surface $AlPO_4$ to form $AlPO_4 \cdot nH_2O$; (a′) hydration of surface $Al_2O_3 \cdot nH_2O$ to $Al_2O_3 \cdot mH_2O$, where $m > n$; (b) nucleation and growth of a hydrated phase, AlOOH; (c) dissolution of $AlPO_4 \cdot nH_2O$ without hydration of underlying Al_2O_3; and (d) dissolution of $AlPO_4 \cdot mH_2O$, followed by hydration of Al_2O_3.

$\Delta y = -y(n+1)\delta$, and, accordingly,

$$\tan\alpha = \frac{\sqrt{3}}{1+\frac{2}{y}\left[x-\frac{1}{n+1}\right]}. \quad (5)$$

This tangent defines the tie-line connecting the initial point (x, y, z) and the end-point corresponding to $Al_2O_3 \cdot nH_2O$ on the behaviour diagram (Path b in Fig. 7). The composition of each point on the tie-line is a linear combination of the two end points. When $n = 1$, a special situation arises, and the end-point corresponds to AlOOH.

4.3. Dissolution of $AlPO_4$ or $AlPO_4 \cdot nH_2O$ without hydration of the underlying Al_2O_3

In this case, more Al_2O_3 is exposed, $\Delta x > 0$, and $AlPO_4$ and H_2O decrease proportionally, $\Delta z = n\Delta y < 0$ and $\tan\alpha = -\sqrt{3}/(2n+1)$. The surface composition evolves along a tie-line connecting the initial points and that corresponding to Al_2O_3 (Path c in Fig. 7).

4.4. Dissolution of $AlPO_4$ or $AlPO_4 \cdot nH_2O$ followed by hydration of the Al_2O_3

This case can be considered a combination of the reactions in Sections 4.2 and 4.3. The initial and final compositions are the same as that in Section 4.2, but the phosphate concentration initially decreases more rapidly in this example. The composition of the surface evolves along a curve bonded by Paths b and c and Al_2O_3–H_2O (Path d in Fig. 7). The deviation of this curve from the straight line is a function of the relative kinetics of the two mechanisms. In the limiting case, i.e., where the dissolution of PO_4^{3-} proceeds slowly (i.e., it is the rate-limiting step) and the hydration of the exposed surface follows quickly, the evolution of the surface oxide composition would be very similar to that of Path b. These are, in fact, the expected relative rates of dissolution and hydration and, to distinguish between the two cases, additional measurements are needed. The results of the measurements are discussed below.

Thus, the surface behaviour diagram (given in Fig. 4) and the above analysis suggests a three-step model for the hydration process of the PAA oxide.

In the first step, the surface $AlPO_4$ layer hydrates to form $AlPO_4 \cdot nH_2O$. This initial step may be regarded as a precursor activity because it can occur readily during storage or as a result of improper drying of the sample and can be easily reversed. Furthermore, no change of oxide morphology can be detected by the STEM. This step is characterized by a horizontal evolution in the behaviour diagram.

Since the evolution of the surface composition during the second step of the hydration process is directly toward AlOOH, the hydration must proceed by either (i) the nucleation and growth of AlOOH without dissolution of the surface phosphate layer or (ii) a slow dissolution of phosphate followed by rapid hydration of the exposed Al_2O_3. We cannot distinguish between the two possibilities with our surface composition data alone, but the following two arguments suggest that the second reaction is applicable. First, the formation of AlOOH requires the availability in solution of aluminium ions that must come from dissolution and hydrolysis of Al_2O_3, i.e., the protective phosphate layer must dissolve or become discontinuous to make the aluminium ions available. Second, and more demonstrably, Auger depth profiling indicates that less than one-fifth of the phosphate originally present (see Fig. 8) is detected throughout the boehmite layer of a hydrated surface (see Fig. 9). Therefore, it is proposed that phosphate dissolution plays an important role in the hydration of PAA surfaces. In fact, during the second step it appears to be the rate-controlling process.

The third hydration step comprises the nucleation and growth of the bayerite phase, $Al(OH)_3$. The surface composition evolves along the Al_2O_3–H_2O tie-line, i.e., the normal hydration path of pure Al_2O_3. Although SEM micrographic and X-ray diffraction analysis indicate bayerite crystallites on top of the boehmite, the results are insufficient to determine whether the bayerite is converted from the boehmite via dissolution–redeposition or by simple nucleation in the presence of the boehmite.

All the behaviour diagrams shown up to now have described the near-surface region of the samples. As mentioned earlier, the photoelectrons measured to generate the behaviour diagrams have a mean free path of 4 to 5 atomic layers. Consequently, the signal from the outermost surface layer is only one-fourth of the total signal; the behaviour diagrams thus indicate the depth of the hydration products. We can adjust for this effect to derive the hydration behaviour diagram for the outermost surface layer only (see Fig. 10). It shows

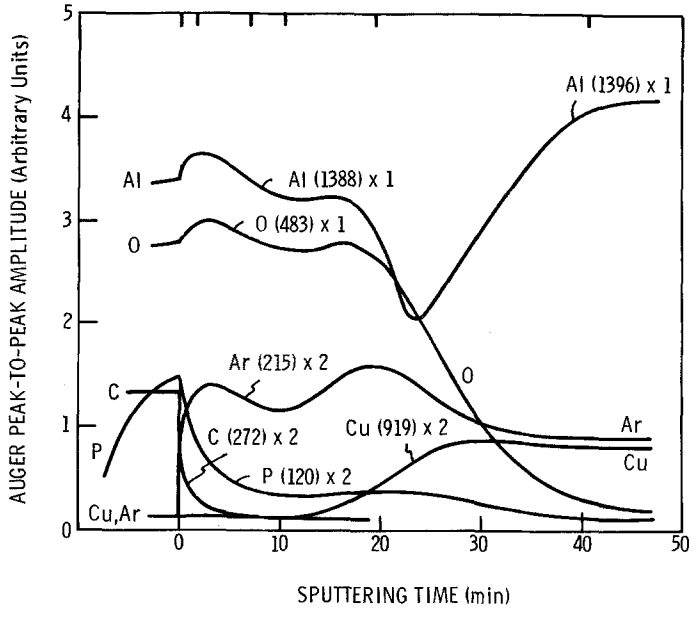

Figure 8 Auger depth profile of unhydrated PAA oxide in 2024 aluminium. The numbers in parentheses are the kinetic energies of the Auger transitions used. The relative scale for each transition is given by the number following the parentheses.

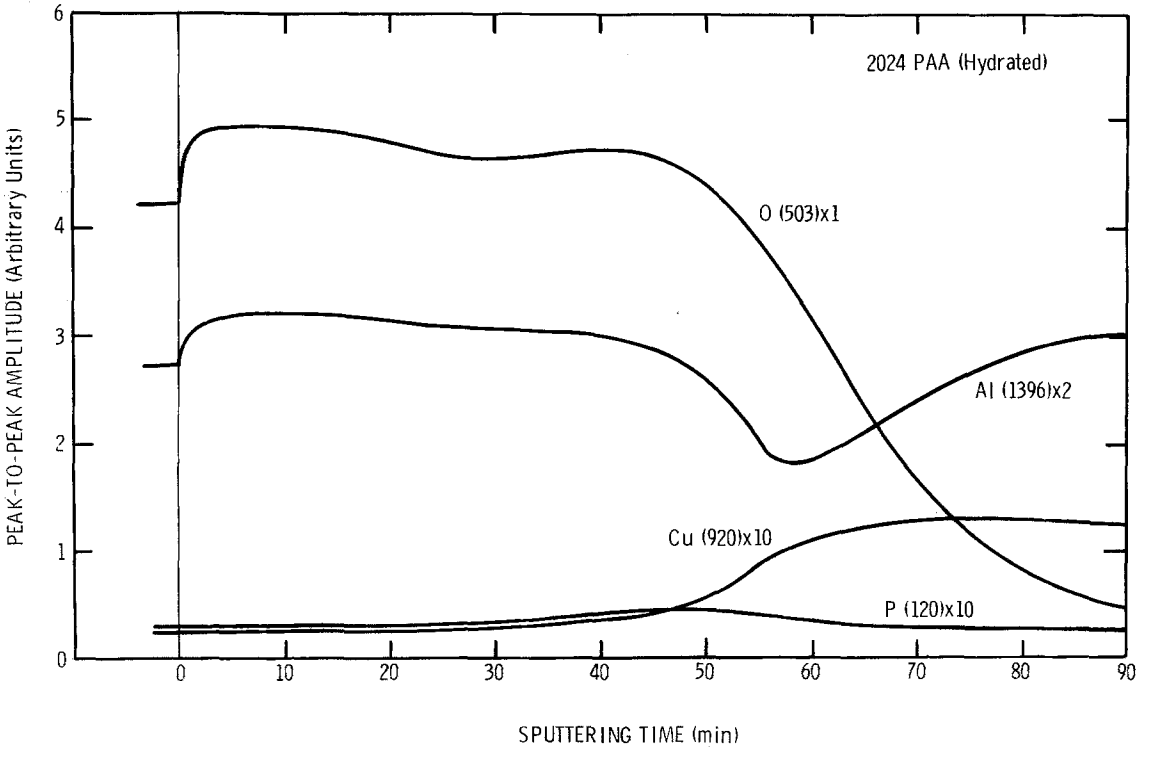

Figure 9 Auger depth profile of PAA oxide on 2024 aluminium hydrated in 100% relative humidity at 50° C for 73 h. The numbers in parentheses are the kinetic energies of the Auger transitions used. The relative scale for each transition is given by the number following the parentheses (note that the oxygen transition is different from that used for Fig. 8). The phosphorus signal in the oxide is barely detectable above the noise level given by the copper signal in the oxide and the phosphorus signal in the metal.

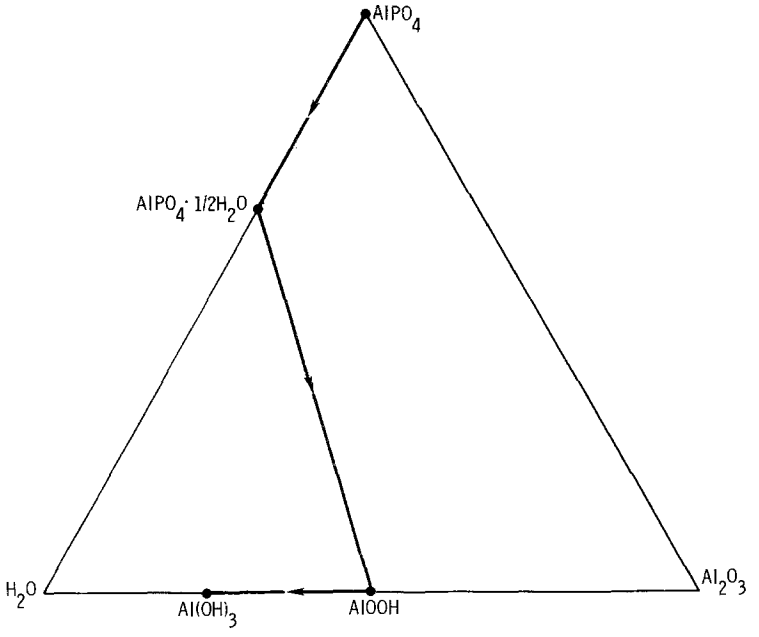

Figure 10 Surface behaviour diagram of the outermost surface layer of 2024 aluminium hydrated in 100% relative humidity at 50° C. Hydration consists of three steps: a precursor hydration of the $AlPO_4$, the nucleation and growth of AlOOH and the nucleation and growth of $Al(OH)_3$.

an initial monolayer of $AlPO_4$ which adsorbs water to become $AlPO_4 \cdot nH_2O$ ($n \leqslant 1$). Hydration continues with the nucleation of an AlOOH surface layer. Finally, the surface hydrates further to become $Al(OH)_3$.

5. Conclusions

By using surface behaviour diagrams to trace the evolution of the surface composition of a phosphoric-acid-anodized aluminium adherend exposed to water-vapour-saturated atmosphere, it has been shown that the hydration process proceeds in three stages. The first stage involves the adsorption of water by the monolayer of $AlPO_4$ present on the surface. This adsorption occurs readily during storage, but is reversible and involves no morphological change. In the second stage, the $AlPO_4$ monolayer slowly dissolves and the exposed Al_2O_3 quickly hydrates to boehmite AlOOH. It is this rate-limiting dissolution of the protective phosphate layer that gives the PAA aluminium surface its superior hydration resistance and its long-term adhesive-bond durability. In the final hydration step, the surface hydrates further to become bayerite $Al(OH)_3$.

This three-step nature of the hydration process became evident only upon plotting the surface composition, as a function of time, on the $AlPO_4$–Al_2O_3–H_2O surface behaviour diagram. Since changes in the composition of surfaces as a function of time, temperature, and other variables can be easily visualized on the appropriate surface behaviour diagrams, it is expected they will become a generally useful tool to study surface reactions.

Acknowledgements

We gratefully acknowledge the technical assistance of Mr R. C. Butler and valuable discussions with Dr J. M. Chen and Mr D. K. McNamara. We also thank the Air Force Office of Scientific Research (AFOSR) for sponsoring this study under contract number F 49620–78–C–0097.

References

1. J. D. VENABLES, D. K. McNAMARA, J. M. CHEN, T. S. SUN and R. L. HOPPING, *Appl. Surface Sci.* **3** (1979) 88.
2. H. W. EICHNER and W. E. SCHOWALTER, Forest Products Laboratory, Madison, WI, Report number 1813 (1950).
3. G. S. KABAYASKI and D. J. DONNELLY, Boeing Corporation, Seattle, WA, Report number D6-41517, February (1974).
4. N. W. ROGERS, U.S. Patent number 3,414,489.
5. J. D. VENABLES, D. K. McNAMARA, J. M. CHEN, B. M. DITCHEK, T. I. MORGENTHALER, T. S. SUN and R. L. HOPPING, Proceedings of the 12th National SAMPE Symposium, Seattle, Washington, October 1980 (SAMPE, Azusa, California, 1980) p. 909.
6. T. S. SUN, J. M. CHEN, J. D. VENABLES and R. HOPPING, *Appl. Surface Sci.* **1** (1978) 202.
7. P. W. PALMBERG, *J. Vac. Sci. Technol.* **12** (1975) 379.

8. D. MENETRIER, I. JAWED, T. S. SUN and J. SKALNY, *Cement Concrete Res.* 9 (1975) 473.
9. C. D. WAGNER, W. M. RIGGS, L. E. DAVIS, J. F. MOULDER and G. E. MUILENBERG, "Handbook of X-ray Photoelectron Spectroscopy" (Perkin–Elmer Corp., Physical Electronics Division, Eden Prairie, MN, 1979).
10. T. S. SUN, D. K. McNAMARA, J. S. AHEARN, J. M. CHEN, B. M. DITCHEK and J. D. VENABLES, *Appl. Surface Sci.* 5 (1980) 406.
11. J. S. AHEARN, T. S. SUN, C. FROEDE, J. D. VENABLES and R. L. HOPPING, *SAMPE Quart.* 12 (1980) 39.
12. W. VEDDER and D. A. VERMILYEA, *Trans. Faraday Soc.* 65 (1969) 561.
13. J. P. O'SULLIVAN, J. A. HOCKEY and G. C. WOOD, *ibid.* 65 (1969) 535.
14. D. R. PENN, *J. Electron Spectrosc. Relat. Phenom.* 9 (1976) 29.
15. D. A. VERMILYEA and W. VEDDER, *Trans. Faraday Soc.* 66 (1970) 2649.
16. J. S. HEARN, G. D. DAVIS, T. S. SUN and J. D. VENABLES, Proceedings of the Symposium on Adhesion Aspects of Polymeric Coatings, Minneapolis, May 1981, to be published.

Received 21 October
and accepted 10 November 1981